Charged Particle Identification in Electron Scattering Experiments with CLAS

V. Burkert [a], H. Egiyan [d] L. Elouadrhiri [a,b], K. Loukachine [c], E. Smith [a], S. Stepanyan [a,b]

[a] *Thomas Jefferson National Accelerator Facility, Newport News, VA 23606*

[b] *Christopher Newport University, Newport News, VA 23606*

[c] *Catholic University of America, Washington DC, 20064*

[d] *College of William and Mary, Williamsburg, VA 23185*

Abstract

We describe the charged particle identification technique used in CLAS, the CEBAF Large Acceptance Spectrometer at Jefferson Lab. Particle identification is based on time-of-flight and momentum measurements. The best results are obtained when the event start time is synchronized with the accelerator RF signal and corrected for measurement uncertainties. It is shown that this method allows identification of pions, kaons, protons and deuterons and cleanly separates (at greater than 3σ) pions from protons up 3 GeV/c and pions from kaons up 1.5 GeV/c, respectively. It is also demonstrated that combining TOF with energy losses measurements allows identification of light nuclear fragments such as ^3H and ^3He.

Preprint submitted to Elsevier Preprint *2 May 2002*

1 Introduction

The CEBAF Large Acceptance Spectrometer (CLAS) [1] at Jefferson Lab is designed to measure multi-particle final states. It is based on six iron-free superconducting coils that generate a toroidal magnetic field in between. Each of six gaps between the coils is equipped with a set of drift chambers (DC) [2] and scintillator counters (SC) [3] from 10^o to 145^o in polar angle, and Cherenkov counters (CC) [4] and electromagnetic calorimeters (EC) [5] from 10^o to 45^o.

The identification of charged particles in CLAS is an important part of the physics program. It relies on the particle momentum, its charge and the path length measured in the DC system, and the time-of-flight from the target to the SC plane. Precise time measurements are critical for particle identification (PID). In order to improve the time measurements in the off-line analysis, synchronization of an event start time with the highly stabilized accelerator radio frequency (RF) time is used. Synchronization of the CLAS TOF time with the RF signal was used initially for the calibration of time offsets between scintillator paddles using electrons and pions [6] and for time calibration of CLAS tagging system [7]. This resulted in an overall resolution of $\sigma \sim 140$ *psec* (sigma). Due to the high stability and suitable time structure of the beam, this method provides significant improvements in particle identification.

2 Time-of-flight measurement with CLAS

Each sector of CLAS is instrumented with four planes of scintillator paddles. A total of 288 SC paddles (48 in each sector) cover the full acceptance range of CLAS. Scintillator strips have variable length from 30 *cm* to 400 *cm* and approximately 5 *cm* $\times$ 20 *cm* cross section. Detailed description of the construction and the characteristics of SC can be found elsewhere [3].

The scintillation counters are designed to have a time resolution in the order of 150 *psec*. In order to achieve the best performance in time and amplitude measurements, each scintillator strip is read out with PMT's from both ends. After conversion of the TDC value for a single PMT to the time and after applying time walk and time delay corrections, the mean value of the measured times of both PTM's is calculated. In this way, the dependence on the hit position along the strip is excluded, and the remaining components in the obtained time are:

$$t_i^{SC} = t_i^{ToF} + t_{St} \tag{1}$$

Here t_i^{ToF} is the time-of-flight from the production vertex to the detector element for a particle and t_{St} is the event start time (trigger time). The event start time contains large uncertainties due to the fluctuations of propagation time of the trigger signal. For determination of t_i^{ToF} in (1) the event start time needs to be determined from event analysis not including time information.

In electron scattering, every event is required to have an electron. The electron candidate is found using drift chamber hit-based momentum reconstruction, shower profile and energy deposition in the forward electromagnetic calorimeter and hits in the Cherenkov and the scintillator counters. After an electron candidate is found the event start time (at the target) can then be calculated as:

$$t_{St} \;=\; t_e^{SC} \;-\; \frac{R_e}{v_e} \tag{2}$$

Here t_e^{SC} is the measured time for the electron, R_e is the path length to the SC plane, and v_e is the electron velocity.

If t_{St} is defined, the time-of-flight for each particle in the event can be calculated from (1). The uncertainties in t_i^{ToF} are due to the time resolution of a particular SC strip, where particle i is detected, and the uncertainties in determination of the event start time, t_{St}. As was mentioned, average time resolution of individual strip is expected to be around 150 *psec*. Average accuracy of path length measurements is better than 1 *cm*. Therefore the main contribution to the resolution of TOF is from uncertainties in the time measurements.

3 Correction of event start time

The CEBAF accelerator at Jefferson Lab is based on superconducting accelerating cavities operating at a highly stabilized frequency of 1.497×10^9 sec^{-1} [8]. Electrons ride on the crest of the RF field wave with a bunch length of a few picoseconds. Every third bunch of electrons is directed towards one of the three experimental areas, creating a trail of electrons equally spaced by 2.004 *nsec*.

The bunch-to-bunch separation is large enough to be resolved by the CLAS TOF system using scattered electrons. The bunch width is very narrow compared to the intrinsic time resolution of SC. Therefore the beam bunch position can be used to remove measurement uncertainties from the event start time in (2). To make this correction, the prescaled (1/40) RF pulse from the RF oscillator was timed on fast TDC.

The prescale factor was chosen such that there was always an RF pulse in the time window

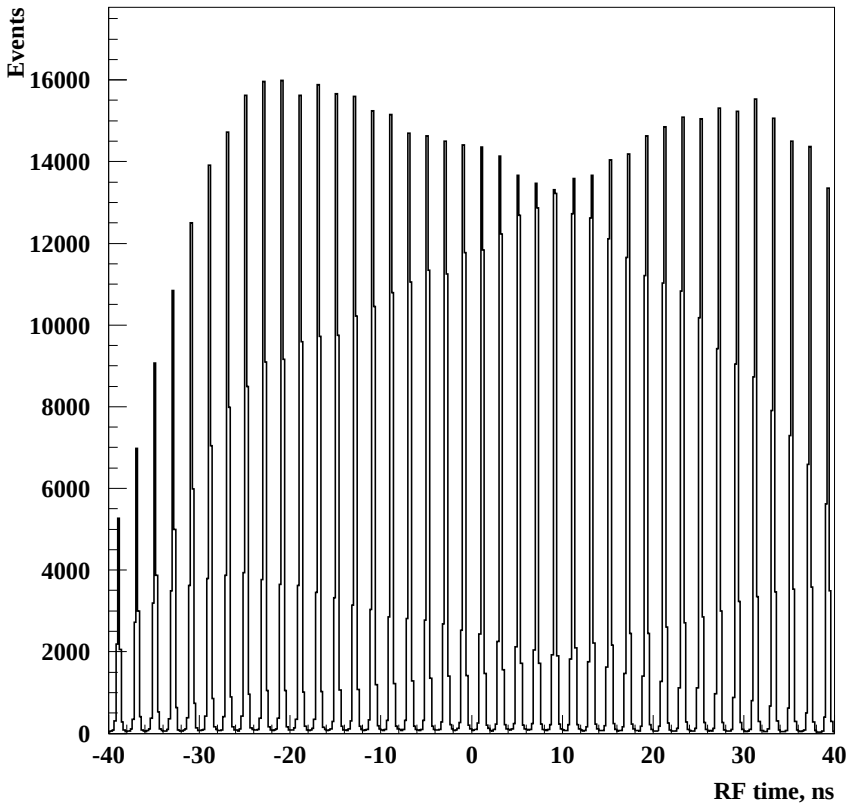

Fig. 1. The beam time structure as seen in the difference of electron start time and RF time.

of the TDC. Relative time measured in this case (in analogy to (1)) is:

$$t_{RF} \;=\; n \times \delta t^{c}_{RF} \;+\; t^{o}_{RF} \;+\; t_{St} \tag{3}$$

where δt^{c}_{RF} is the RF structure constant of 2.004 $nsec$ and n is an integer with random value but with an upper limit as defined by the trigger time window. t^{o}_{RF} is a parameter that is related to the time-of-flight of electrons from RF separator to the target. This parameter is determined during the calibration and remains quite stable if the beam tune is not changed. (Correction due to target length is done event-by-event bases using the vertex position reconstructed by tracking).

If the event start time is removed from (3) using the expression (2), the resulting distribution will repeat the beam time structure with a constant time offset t^{o}_{RF}.

In Figure 1, a typical distribution of the measured RF time is shown after subtraction of the

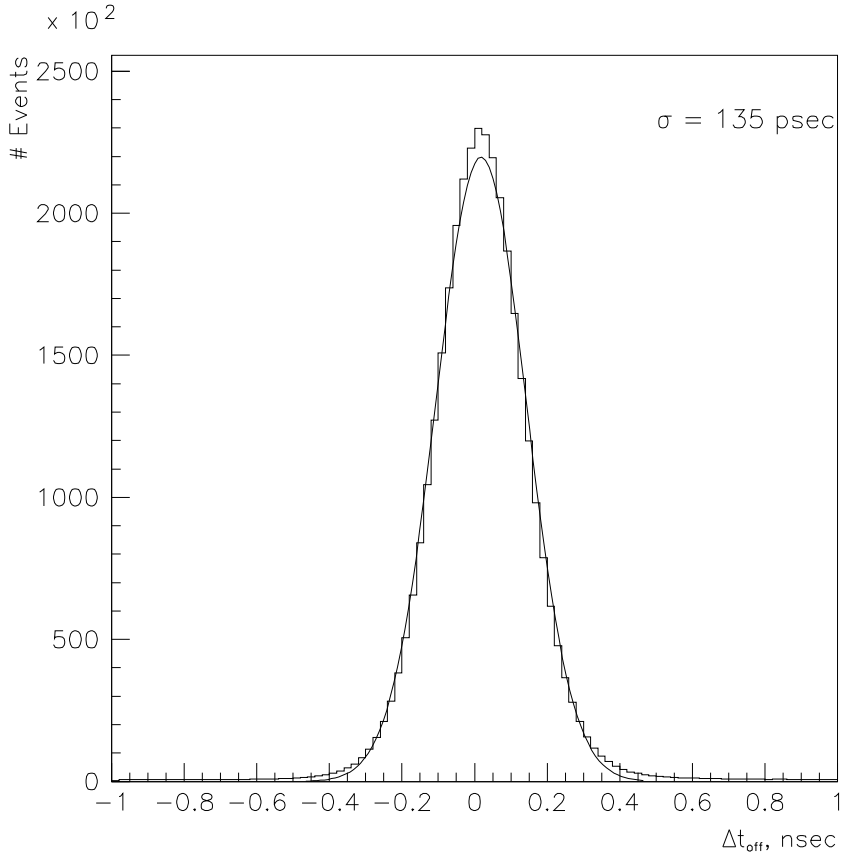

Fig. 2. Distribution of RF corrections obtained after taking the modulus of δt^c_{RF} from the difference of the start time and the RF time.

event start time. Although peaks are 2.004 *nsec* apart, they are much wider ($\approx$ 140 *psec*) than the beam bunch (few picoseconds). The absolute positions of peaks are defined by the parameter t^o_{RF}. The widths of the distribution in each peak in Figure 1 are mainly due to the uncertainties in the start time. Real interaction occurs at the peak position and therefore uncertainties can be reduced.

To get the correction, all peaks in Figure 1 were folded on top of each other by taking the modulus of δt^c_{RF} from the difference in the RF time in (3) and the start time from (2):

$$\Delta t_{Off} \;=\; MOD(t_{RF} - t_{St}, \delta t^c_{RF}\;) - \frac{\delta t^c_{RF}}{2}. \tag{4}$$

In Figure 2 a typical distribution of Δt_{Off} is shown. The parameter t^o_{RF} is chosen such that the Δt_{Off} is centered at "0" and therefore the value of Δt_{Off} is the correction that must

be applied to the start time.

4 Particle identification

After determination of the time-of-flight from (1) and (2), the velocity of the particle can be calculated using the path length as measured by tracking:

$$\beta_i \;=\; \frac{R_i}{c \times t_i^{ToF}}. \tag{5}$$

Here R_i is the path length and t_i^{ToF} is the time-of-flight after subtraction of the RF-corrected event start time. The particle identification procedure involves the minimization of $\beta_i - \beta_a$, where β_a is calculated as:

$$\beta_a \;=\; \frac{p_i}{\sqrt{p_i^2 \;+\; m_a^2}} \tag{6}$$

for each possible candidate particle type a with mass m_a (e.g., proton, pion, kaon, deuteron etc.). In (6) p_i is the measured momentum.

Figure 3 shows β_i versus p_i for positive particles. The data are from measurements of electron scattering off a carbon target at 4.4 GeV. Bands for protons, pions, kaons and deuterons are clearly visible. At low momenta bands for e^+ and ^3H are visible as well.

The quality of particle identification depends on the accuracy of the β and momentum measurements. Distributions of $\delta\beta_a = \beta_i - \beta_a$ were analyzed for each particle type. In Figure 4 $\delta\beta_p$ is displayed versus momentum. The central band corresponds to the protons. The band was fitted with a Gaussian function in small momentum bins. The average sigma of the $\delta\beta_p$ distribution was found to be $\sigma_{\delta\beta} \approx 0.01$. Similar fits were made for other particles as well (see Figure 5).

The mean values of the corresponding distributions for heavier particles are shifted from zero, indicating possible systematic shifts in the absolute determination of the path length as well as uncertainties in the time walk corrections.

Figure 6 summarizes the fit results. The widths of the $\beta(p)$ lines for each particle on the plot correspond to 1σ of the experimentally obtained distributions.

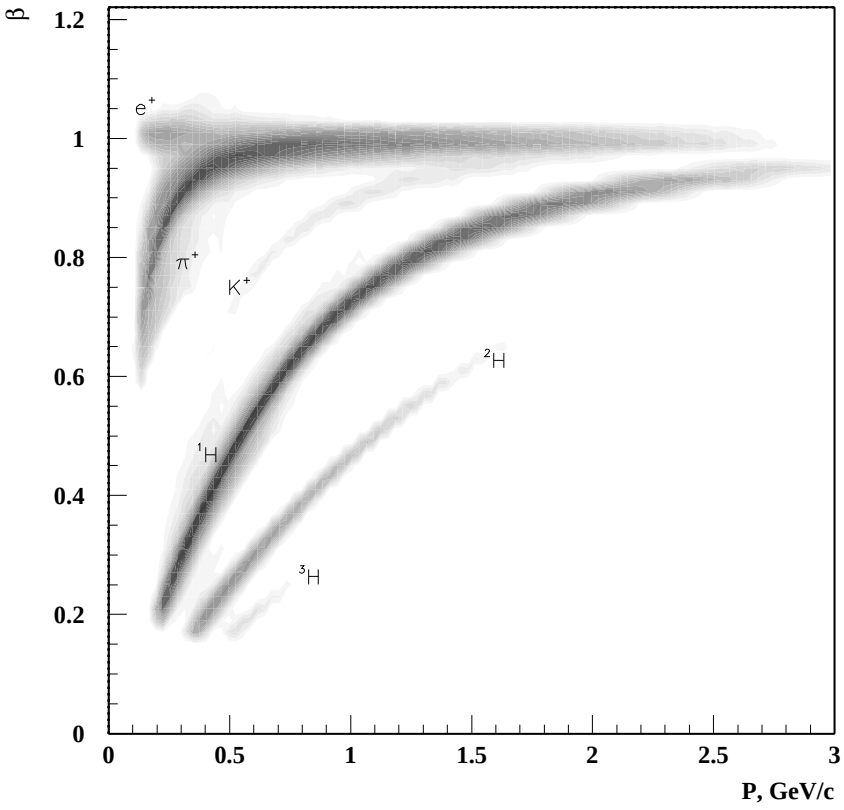

Fig. 3. The dependence of β from (5) on momentum for positively charged particles in the scattering of 4.4 GeV electrons off a carbon target.

4.1 Separation of charged hadrons

As follows from Figure 6, protons and deuterons can be separated in the full momentum range, protons and kaons for momenta up to $2GeV/c$. The limitations are in pion-kaon and pion-proton separation.

The bulk of particles reconstructed in CLAS are charged pions and protons. There is a 3σ separation for pions and protons up to 3 GeV/c. There is also greater than 3σ separation of pions and kaons with momenta up to 1.5 GeV/c [1].

Light nuclear fragments such as ^3H or ^3He can be identified using time measurements with energy loss information. This is discussed in Section 6.

[1] In addition the kaon identification can be improved by using kinematical and physics constraints.

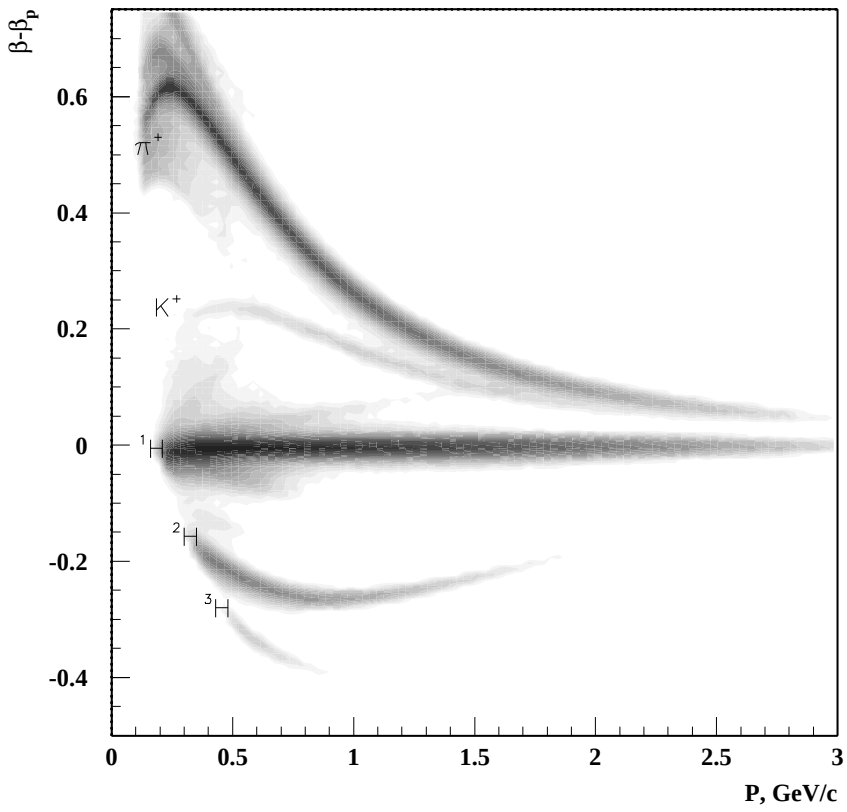

Fig. 4. The distribution of $\beta - \beta_p$ as a function of momenta for positively charged particles. The band along the $\beta - \beta_p = 0$ corresponds to the protons.

4.2 Pion-electron separation at low momenta

Due to the open geometry of CLAS and the nature of the electromagnetic interaction, there is a significant flow of electrons and positrons into the detector volume. The bulk of those pairs are from radiative photons, converted into the e^+e^- in the target region, and Dalitz decay of $\pi^o \to e^+e^-\gamma$, and typically have relatively low energy. Most of produced particles, especially e^+, get deflected to the large angle region of CLAS and only TOF methods can be used for identification and for pion/electron(positron) rejection.

The distributions of $\delta\beta_\pi$ for negative and positive particles are shown in Figure 7. There is a clean separation between pions and electrons (positrons) for momenta up to 400 MeV/c. This gives a significant reduction in the number of e^+ or e^- misidentified as π^+ or π^-, respectively. One also notices that for momenta below 0.3 GeV/c the $\mu^{+(-)}$ band is cleanly

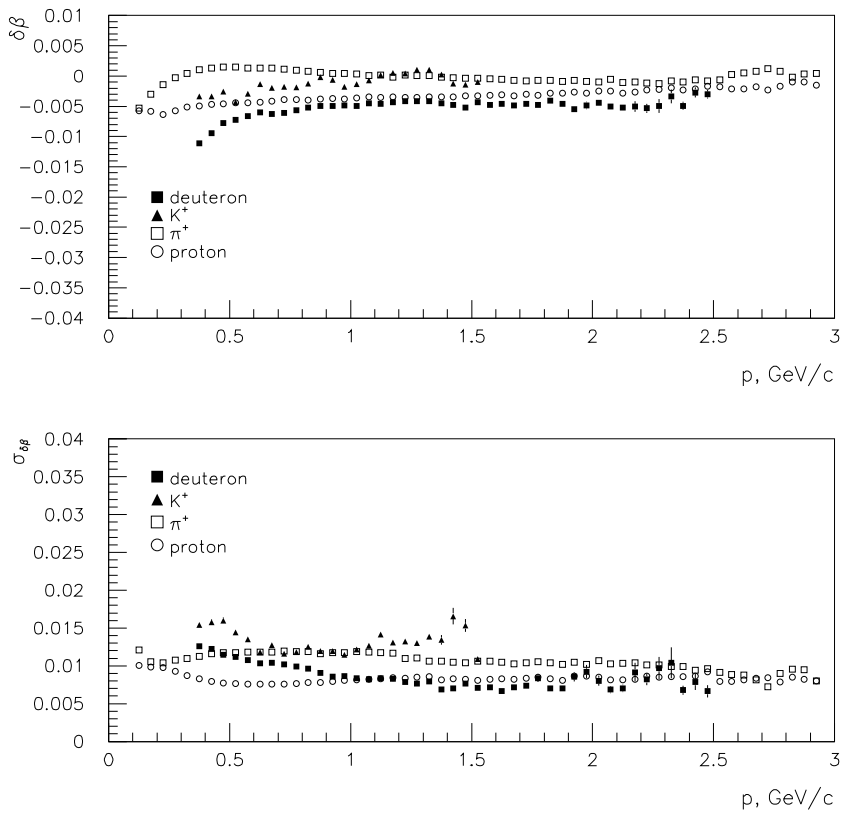

Fig. 5. Dependence of the mean value and σ of the $\delta\beta$ distributions on momenta for various particle species.

separated from pions as well.

5 Bunch crossing and accidentals

Although the duty factor of the electron beam is very high and the luminosity used in CLAS quite low, there are still accidental coincidences, when particles produced from different beam bunches may be detected in the same event. This may cause a misidentification of protons from previous bunches as pions or kaons.

In order to estimate the fraction of protons from other beam bunches in an event, and to estimate the level of overall miscalibration, protons were identified using the energy loss in SC in the momentum range from 0.4 GeV/c to 1 GeV/c. Then the time difference of the

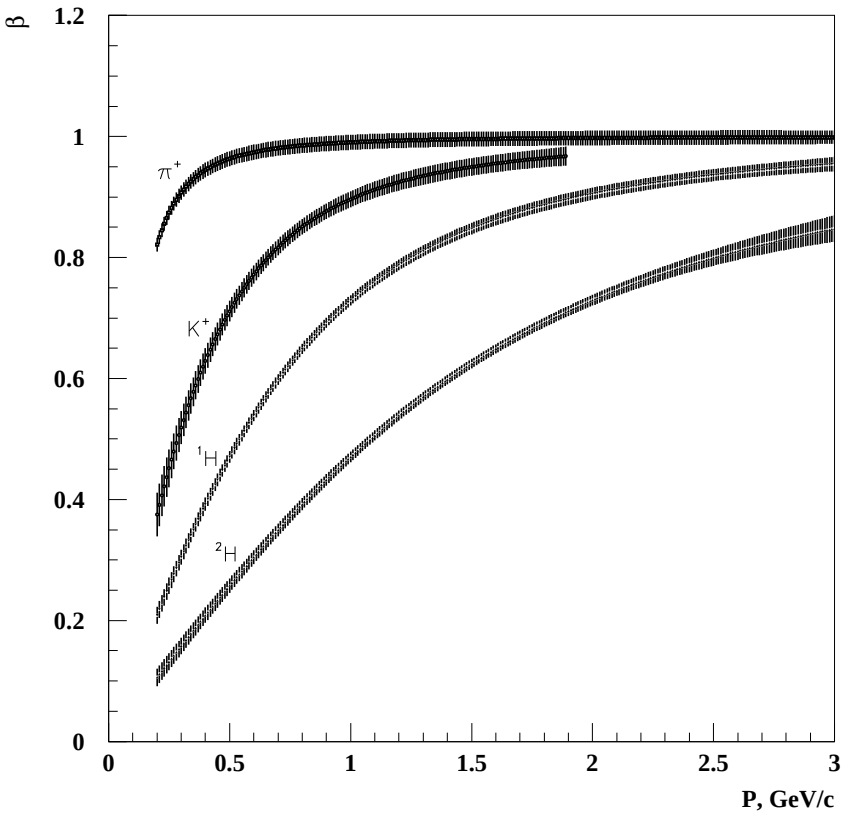

Fig. 6. β vs momenta plot for various particles. Width of bands corresponds to sigma of experimentally obtained distribution.

measured and estimated time-of-flights is:

$$\delta t_p \;=\; R_i \times (\frac{1}{c\beta_p} - \frac{1}{c\beta_i}) \tag{7}$$

where R_i and β_i are the measured path length and beta of the particle, respectively. β_p is calculated using the measured momentum, assuming the particle is a proton. In Figure 8, the distribution of δt for a momentum range from 0.6 GeV to 1 GeV is shown.

The peaks reflect the bunch structure of the electron beam and are visible due to the applied RF correction to the start time. The central peak corresponds to protons identified as being from the same beam bunch as the detected electron. There are two main sources contributing to the events from neighboring peaks. First, particle can be assigned to a different RF bunch than the electron due to time smearing. This leads to a $\sim\ 10^{-2}$ population of particles in

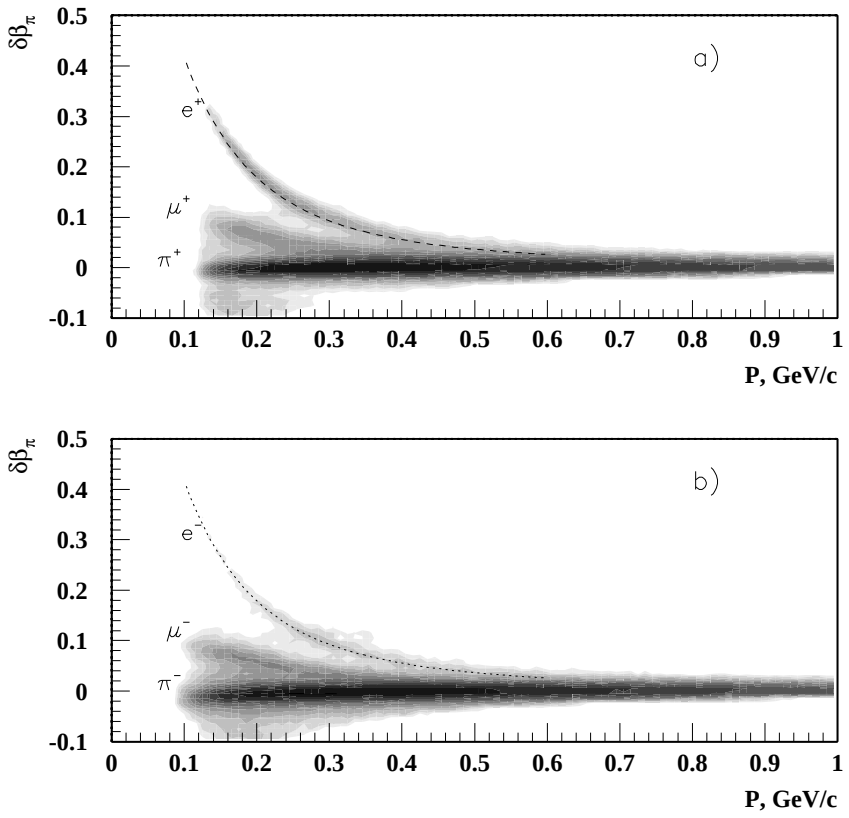

Fig. 7. The distribution of $\beta - \beta_\pi$ as a function of momenta for positive (a) and negative (b) particles.

the bunches left and right from the central peak. This can be easily corrected for events with more than one particle in addition to the electron. The second source is due to the detection of particles from beam bunches different from the interaction bunch, as defined by the triggering electron. These particles will be uniformly distributed in the time window of the event. This contribution is of the order of 10^{-4}. Although the bulk of particles in the flat shoulder are due to accidentals, there are also some contributions to the flat background from miscalibrated or malfunctioning detector elements.

6 Identification of light nuclear fragments

The amount of material in the way of particles in CLAS is low enough ($\sim 1\ g/cm^2$) to allow low energy protons and light nuclear fragments to pass through the entire detector and

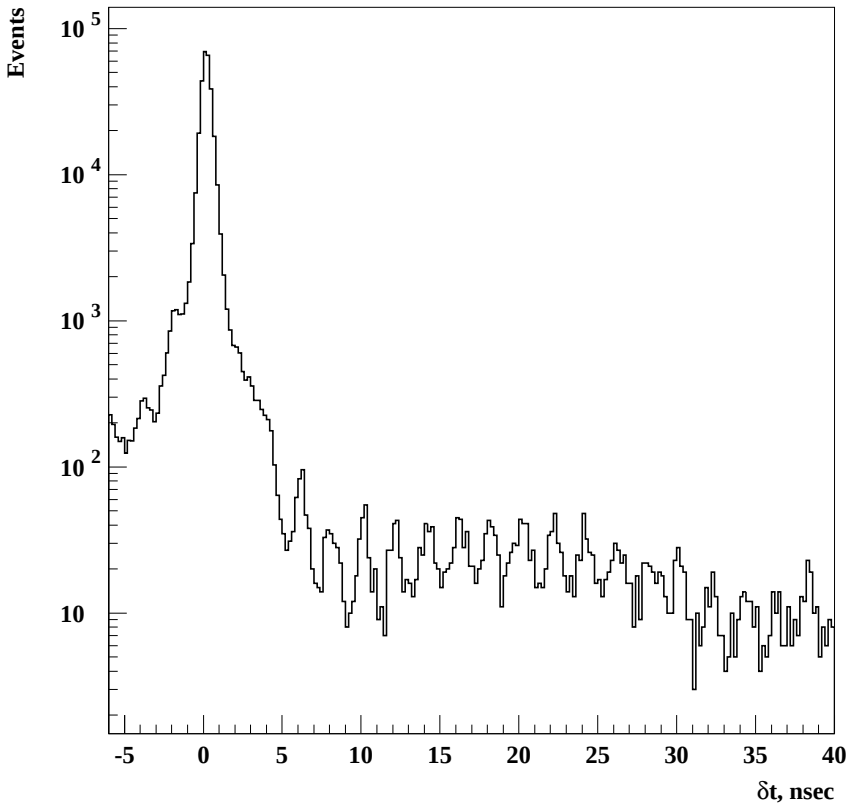

Fig. 8. The distribution of measured and calculated times for protons selected with $\frac{\delta E}{\delta X}$ cut.

be detected. From Figure 3 one can see that the momentum acceptance range for protons begins at 0.25 GeV, for deuterons at $\sim$ 0.3 GeV/c, and for ^3H at $\sim$ 0.4 GeV/c.

Although time-of-flight measurements alone allows resonable identification of frugments such as ^2H and ^3H, identification, in general, can be improved by using also information on energy loss in the TOF bar. For example, doubly charged ^3He deposits significantly more energy in the scintillators than other singly charged particles. This can be used to enhance and improve identification of ^3He. In Figure 9, the energy losses for positive particles are shown as a function of momentum. Bands of minimum ionizing particles and protons are clearly seen in the range of energy losses up to 100 MeV, as well as a band of deuterons.

In the range of energy losses above $\sim 80MeV$ there is a distinct band corresponding to ^3He. This contribution is clearly visible in the mass spectra when applying a cut on the energy loss. The mass distribution of positive particles calculated using measured momentum and beta is shown in Figure 10. A cut to the energy loss in the SC enhances the peak near

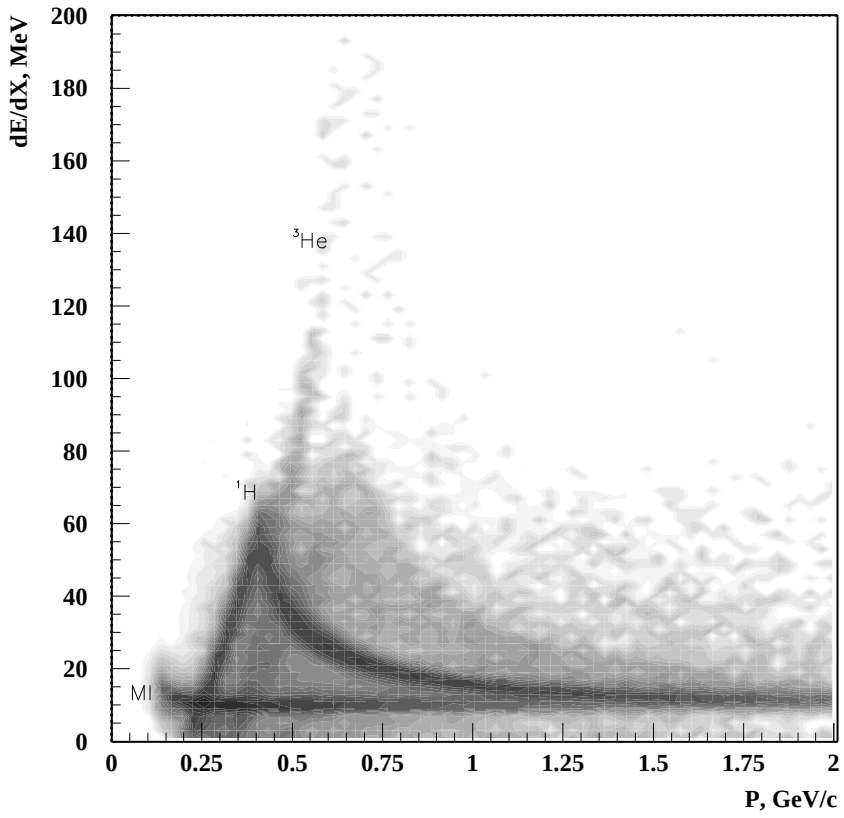

Fig. 9. The distribution of energy losses of positive particles vs momenta.

1.4 GeV/c^2, which corresponds to ^3He nuclei. The mass peak is at the half of the nominal mass since in the momentum reconstruction a unit charge is assumed for all tracks.

7 Conclusion

The charged particle identification technique used in CLAS is based on time-of-flight and momentum measurements. The synchronization of the measured time in the CLAS TOF system with the accelerator RF signal allows a significant (25 % to 35 %) reduction of the uncertainties in the time measurements by correcting the event start time with the peak position of the beam bunch. Using the corrected times allows separation of pions from protons with momenta up to 3 GeV/c, protons from kaons up to 1.5 GeV/c, and electrons from pions up to 0.4 GeV/c. The combination of TOF and energy losses in the SC allows identification of nuclear fragments such as ^3H and ^3He as well.

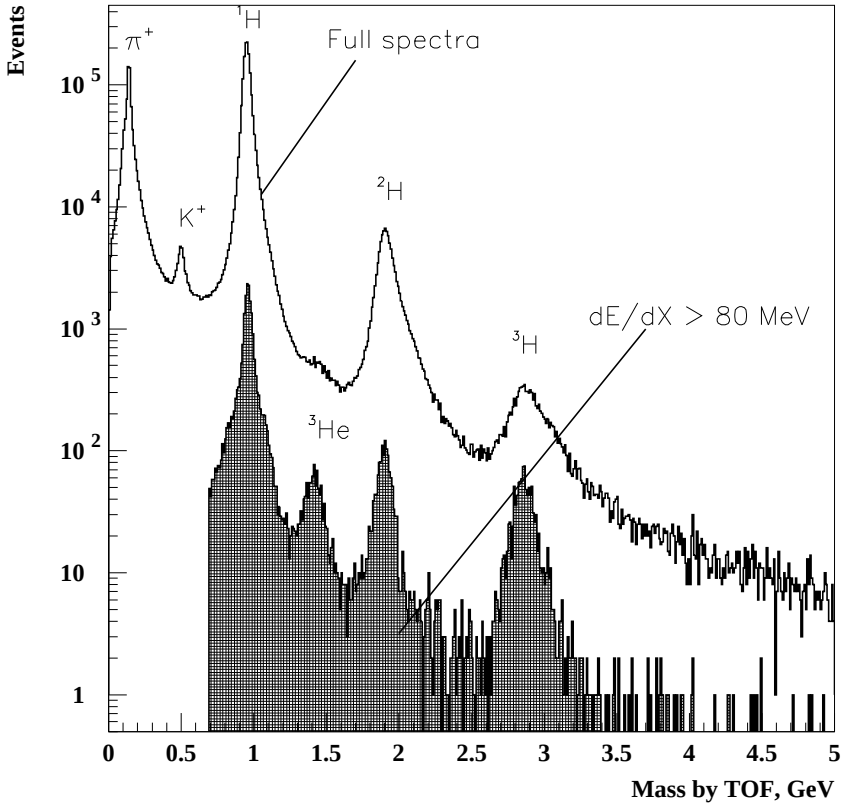

Fig. 10. The mass distribution of positive hadrons calculated using the measured momentum and the β. The open histogram corresponds to the mass distribution of all positive particles. The dashed histogram is the mass distribution after the $\frac{\delta E}{\delta X}$ cut, to enhance the contribution of ^3He.

8 Acknowledgements

The authors wish to thank members of CLAS TOF group: E. Smith, students K. Loukachine, S. Taylor, H. Egiyan for maintaining and calibrating the TOF system, for developing hit reconstruction and calibration algorithms. We grateful to B. Mecking and R. Shumacher for helpful discussions and comments. Graduate students D. Protopopescu, G. Gavalian and H. Aznaurian must be acknowledged for their efforts of calibrating the data that have been used. Also many thanks to E. Anciant, G. Audit, T. Auger, C. Marchand, P. Girard for preparing the electronics for splitting and pre-scaling RF signal, and for useful discussions.

References

[1] B. Mecking et al., *CLAS detector*, In preparation, to be submitted to Nucl. Instr. and Meth..

[2] M.D. Mestayer et al., *The CLAS drift chamber system*, Nucl. Instr. and Meth. **A449** (2000), p81.

[3] E.S. Smith et al., *The time-of-flight system for CLAS*, Nucl. Instr. and Meth. **A432** (1999), p265.

[4] *The Cherenkov counter system for CLAS*, In preparation, to be submitted to Nucl. Instr. and Meth..

[5] L.C. Smith et al., *The CLAS forward electromagnetic calorimeter*, Accepted for publication in Nucl. Instr. and Meth..

[6] L. Elouadrhiri et al., *Charge Particle Identification in CLAS*, **CLAS Note 98-004**.

[7] E. Anciant et al., *Tagger hit reconstruction software and tagger calibration overview*, **CLAS Note 99-004**.

[8] C. Hovater et al., *The CEBAF RF Separator System*, **JLAB-ACC-98-18**.